Metabolic alterations in a slow-paced model of pancreatic cancer-induced wasting

Elisabeth Wyart[1], Simone Reano[2], Myriam Y Hsu[1], Dario Livio Longo[3], Mingchuan Li[1], Emilio Hirsh[1], Nicoletta Filigheddu[2], Alessandra Ghigo[1], Chiara Riganti[4] and Paolo Ettore Porporato[5]

[1]Department of Molecular Biotechnology and Health Science, Molecular Biotechnology Center, University of Torino, Torino, Italy.
[2]Department of Translational Medicine, University of Piemonte Orientale, Novara, Italy and IstitutoInteruniversitario di Miologia (IIM).
[3]Department of Molecular Biotechnology and Health Science, Molecular Imaging Center, University of Torino, Torino, Italy.
[4]Department of Oncology, University of Torino, Torino, Italy. chiara.riganti@unito.it
[5]Department of Molecular Biotechnology and Health Science, Molecular Biotechnology Center, University of Torino, Torino, Italy. paolo.porporato@unito.it

Abstract 167 words.

Cancer cachexia is a devastating syndrome occurring in the majority of terminally-ill cancer patients. Notably, skeletal muscle atrophy is a consistent feature affecting the quality of life and prognosis. To date, limited therapeutic options are available, and research in the field is hampered by the lack of satisfactory models to study the complexity of wasting in cachexia-inducing tumors, such as pancreatic cancer. Moreover, currently used *in vivo* models are characterized by an explosive cachexia with a lethal wasting within few days, while pancreatic cancer patients might experience alterations long before the onset of overt wasting. In this work, we established and characterized a slow-paced model of pancreatic cancer-induced muscle wasting that promotes efficient muscular wasting *in vitro* and *in vivo*. Treatment with conditioned media from pancreatic cancer cells led to the induction of atrophy *in vitro,* while tumor-bearing mice presented a clear reduction of muscle mass and functionality. Intriguingly, several metabolic alterations in tumor-bearing mice were identified, paving the way for therapeutic interventions with drugs targeting metabolism.

Introduction

More than half of cancer patients are suffering from a systemic wasting disorder referred to as cachexia (from Greek "bad condition"), a syndrome strongly affecting the quality of life and prognosis in cancer patients. This syndrome is characterized by unstoppable consumption of adipose and skeletal muscle tissues leading to an excessive body weight loss that cannot be fully reverted by conventional nutritional support[1].

Cancer cachexia is a complex syndrome accounting for multiple organ dysfunction and systemic metabolic deregulations[2]. Cachectic patients experience symptoms ranging from anorexia, elevated inflammation, insulin resistance, and increased energy expenditure, which ultimately promote malaise, fatigue, and impair tolerance to chemotherapy[3], further worsening patients' prognosis. Besides being associated with a poor prognosis, cachexia is estimated to be the direct cause of one-third of cancer deaths[4]. Several tissue dysfunctions emerge during cachexia, such as liver steatosis, fat deposit lipolysis, intestinal dysbiosis, and, most notably, skeletal muscle wasting, which accounts for the steep decrease in quality of life, weakness, and respiratory distress of cancer patients.

Skeletal muscle atrophy is a highly regulated process driven by an unbalance between protein synthesis and degradation. Activation of the ubiquitin-dependent proteasome pathway (UPP), as well as the autophagy-lysosome system, are two important mechanisms leading to increased protein breakdown. This process is orchestrated by a set of genes called *atrogenes,* such as Atrogin-1/MAFbx or Murf1[5]. Compelling evidence shows that impairment of mitochondrial metabolism and increase in mitochondrial ROS are also strongly associated with the cachectic phenotype[6, 7].

Several tumor types, such as lung, gastrointestinal tract, and pancreatic cancer, are emerging as strong promoters of cancer cachexia[8]. In particular, pancreatic ductal adenocarcinoma (PDAC) presents a high penetrance of wasting, a process that seems to occur even in earlier phases of tumor transformation[9]. Despite the burden of cachexia in PDAC, there are still limited experimental models available.

Particularly, our understanding of the biology underlying cachexia is mostly based on the extensively used and well characterized C26 carcinoma model, in which mice are drastically losing muscle and total body weight in a short period[10], thus contrasting with the progressive wasting occurring in the human pathology. It is known that C26 model is associated with high levels of IL6 that play a central role in mediating muscle wasting[11], even though other inducers are probably involved in cachexia. In order to better characterize early stages of cachexia, we established a model of pancreatic cancer-induced cachexia able to promote mitochondrial metabolic alterations and a progressive wasting both *in vivo* and *in vitro*.

Results

Establishment of a slow-paced cancer-induced muscle wasting model.

PDAC is known to induce muscle wasting with high penetrance [3]. Since cancer cachexia is a complex syndrome involving various pathological processes promoting wasting, such as anorexia and chronic inflammation, it is difficult to assess the direct contribution from the tumor. Therefore, we decided to assess the direct role of cancer cells on skeletal muscle atrophy *via* an *in vitro* model of atrophy, thus excluding other systemic confounding atrophic factors, hypothesizing that, in this type of cancer, atrophy can be mediated directly by tumor cell-secreted factors.

To this aim, we took advantage of KPC cells, a stable cell line derived from spontaneous primary tumor arisen in C57BL/6 $KRAS^{G12D}$ $P53^{R172H}$Pdx-$Cre^{+/+}$ (KPC) mouse[12], a genetically modified mouse model known to develop spontaneous wasting[9]. Similarly to other cancer models[13], in our experimental conditions, KPC cells were able to directly promote muscle atrophy *in vitro*. Treatment of C2C12-derived myotubes with 10% KPC cells conditioned media induced a consistent reduction of myotube thickness, similar to that elicited by dexamethasone, used as a positive control of atrophy induction (Figure 1A). Reduction in fiber thickness was associated with higher ROS generation (Figure 1B). A recent report from Michaelis et al.[12] showed that a subcutaneous injection of 5 millions of these cells consistently promotes anorexia, hormonal dysfunctions, and lethal cachexia in 2 weeks. In order to establish a progressive model of wasting, we subcutaneously injected 0.7 million of KPC cells, which is the minimal amount able to consistently induce tumor growth without exacerbating factors such as excessive tumor burden and anorexia. Indeed, 5 weeks after KPC cell injection, neither food intake alteration (Figure 1C) nor macroscopic features of wasting were observed, despite a non-significant trend of decrease in body weight (Figure 1D). Tumor weight at the end of experiment was approximatively 0.6 grams (Figure 1E), while in the other work weight was between 1 and 2 grams[12]. Remarkably, despite the absence of overt signs of cachexia, skeletal muscle functionality, checked by Rotarod evaluation twice a week (not shown), was drastically affected, but only at week 5, the week of the sacrifice. Accordingly, tumor-bearing mice showed reduced muscle performance, as assessed by hanging-wire test[14] (Figure 1F), suggesting muscle deterioration in tumor-bearing animals. Along

with reduced performance in stamina-related assays, mice displayed as well a reduction in grip strength, indicating that also the maximal force developed was reduced (Figure 1G).

Coherently with the decrease in muscle functionality, 5 weeks after KPC injection, mice presented a consistent loss of gastrocnemius mass of roughly 20% (Figure 2A). The decrease was related to a reduction in average fiber size as detailed by histological analysis (Figure 2B-D). Coherently, analysis of fiber cross-sectional area (CSA) distribution highlighted a shift towards smaller areas (Figure 2E). Reduction in muscle mass was not associated with transcriptional regulation of atrogenes Atrogin1, Musa, and Murf1, and of Cathepsin L (Figure 2F-I), nor altered expression of ATG7, BECLIN1, and LC3 in gastrocnemii (not shown). Nevertheless, muscle protein lysates presented increased protein ubiquitination (Figure 2J), indicative of an activation of the UPP. Along with increased protein ubiquitination, we identified higher AMPK phosphorylation, in line with the emerging role of AMPK as a functional player in cancer cachexia[15].

Mice undergoing muscle dysfunction present altered lipid metabolism.

Given the importance of energy metabolism in regulating skeletal muscle mass and functionality[16, 17], we investigated potential alterations of mitochondrial metabolism in the skeletal muscle of KPC-bearing mice. To this aim, we assessed basal complex II activity in gastrocnemii by performing succinate dehydrogenase (SDH) activity assay. Intriguingly, gastrocnemius sections from KPC-bearing animals presented increased complex II activity, as evidenced by the increased concentration of blue tetrazolium salt (Figure 3A). However, this increased activity was not coupled with elevated flux through the electron-transport chain (ETC). Indeed, ETC, as measured by Cytochrome C reduction rate in uncoupled mitochondria, was similar in the two groups (Figure 3B).

While SDH activity supports ETC, it is also part of tricarboxylic acid (TCA) cycle, and it is linked to fatty acids oxidation, allowing ketone bodies generated by acetyl coenzyme A due to excessive fatty acid oxidation, to enter the TCA.

To clarify whether the increased SDH activity was indicative of increased fatty acid oxidation, we measured this metabolic pathway in isolated mitochondria from the gastrocnemius of either control or KPC-bearing mice and we observed a significant increase in fatty acid oxidation in muscles of tumor-bearing mice (Figure 3C), consistent with the increase in complex II activity.

In order to identify if the altered intramuscular lipid oxidation was correlated to a systemic dysregulation during this pre-cachectic process, we performed T_1-weighted Magnetic Resonance Imaging (MRI). Intriguingly, 4 weeks post KPC injection (one week before sacrifice), pre-cachectic mice presented reduced bright hyper-intensity regions, indicative of reduced fat deposits (Figure 3D-E).

Coherently, at the time of sacrifice, KPC-bearing mice presented a significant reduction of inguinal fat tissue mass (Figure 3F). Therefore, we speculated that the reduced fat content might be related to increased fatty acid oxidation, a feature previously associated with cancer cachexia[16] in other tumor types.

High SDH activity[18, 19] and excessive fatty acid oxidation might lead to ROS accumulation[20], ultimately promoting mitochondrial dysfunction[21] and fiber damage. Hence, we investigated the impact of tumor growth on mitochondrial ROS and energetic balance. Mitochondria extracted from KPC-bearing animals had indeed increased ROS (Figure 3G), coupled with reduced ATP (Figure 3H), suggesting that the increased fatty acid oxidation may have a detrimental rather than beneficial effect on mitochondria.

Materials and Methods

Animals

Young adult female (9-12 weeks old) C57BL/6J mice were used. All animal experiments were authorized by the Italian Ministry of Health and carried out according to the European Community guiding principles in the care and use of animals.

Generation of PDAC model

KPC tumor cells were derived from a primary culture of pancreatic tumour cells of the Genetically Engineered Mouse Model of PDAC K-ras$^{LSL.G12D/+}$; p53$^{R172H/+}$; Pdx-Cre (KPC).

0.7x10^6 KPC cells in 200µl PBS were injected subcutaneously into the flank of C57bl/6J mice. Mice were sacrificed 5 weeks after injection, when tumor volume was approaching 5mm of radius.

In vivo assessment of muscular strength

Grip test – An automatic grip strength meter was used to measure the maximum forelimb grip strength of mice. The machine measures the peak resistance force of the mouse while the latter is pulled away from the grid of the device. Each animal was assessed several times and the final value corresponds to the average of 5 repeated force measurements in order to minimize procedure-related variability.

Hanging test – Wire-hanging test was used to assess whole-body muscle strength and endurance. The test was performed as previously described[14]. Briefly, mice were subjected to a 180 seconds hanging test on a wire, during which "falling" and "reaching" scores were recorded. When a mouse fell from the wire, falling score was diminished by 1 and when a mouse reached one of the side of the wire, reaching score was increased by 1. A final score was then established using both falling and reaching scores and was represented in the form of a Kaplan-Meier-like curve; score have been normalized with respect to control.

MRI

Magnetic resonance images were acquired on a 1 Tesla M2 system (Aspect, Israel) equipped with a 30-mm transmitter/receiver (TX/RX) solenoid coil to determine body composition[22]. T_1-weighted Spin-Echo images were acquired with high-resolution whole-body coronal orientation (repetition time/echo time/flip angle/number excitations [TR/TE/FA/NEX] 400 ms/9.5 ms/90°/3; field of view [FOV] 10 cm, matrix 192x192, number of slices: 18, slice thickness: 1.5 mm, in-plane spatial resolution: 521 µm, acquisition time: 4min). All T_1-weighted images were processed by an in-house Matlab-developed script (MATLAB R2008, The MathWorks Inc.). The T_1-weighted image histogram

has three dominating classes, background, lean mass and fat, so the total fat volume was isolated by segmenting the image into three categories by using a k-means clustering algorithm[23, 24].

Gene expression analysis

Gastrocnemii were harvested, frozen in liquid nitrogen, and crushed. Total RNA was extracted using TRIzol reagent (Invitrogen, Carlsbad, CA). cDNA was synthesized from 1000 ng of total RNA using cDNA reverse transcription kits (Applied Biosystems, Foster City, CA). Relative mRNA level was analyzed by real time PCR (ABI 7900HT FAST Real-Time PCR system, Applied Biosystems, Foster City, CA) with TaqMan assays, using the Universal Probe Library system (Roche Applied Science, Penzberg, Germany). 18S gene was used as housekeeping control. The following primers were used: *FBX030 (MUSA1)* F:5'-gagaagccagggtttgagc-3' R: 5'-tcatacagtgtgagtgctgctg-3' ; *FBX032(atrogin 1)* F:5'-agtgaggaccggctactgtg-3' R: 5'-gatcaaacgcttgcgaatct-3' ; *TRIM63 (MuRF1)* F:5'-tgacatctacaagcaggagtgc-3' R: 5'-tcgtcttcgtgttccttgc-3' ; *Cathepsin L* F:5'-caaataagaataaatattggcttgtca-3' R:5'-tttgatgtagccttccataccc-3'.

Western Blot

Protein samples from gastrocnemius were extracted with RIPA lysis buffer (150 mM NaCl, 50 mM Tris-HCl, 0.5% sodium deoxycholate, 1.0% Triton X-100, 0.1% SDS 1 mM EDTA) supplemented with protease and phosphatase inhibitor cocktail (Roche). Protein concentration was determined using BCA protein assay (Thermo Fisher Scientific). Lysates were subjected to SDS-PAGE and then transferred to PVDF membrane for immunoblotting analysis. The following antibodies were used: mono- and polyubiquitin (BML-PW8805, Enzo Life Sciences, 1:1000), p-AMPK (2535, Cell Signaling, 1:1000), β-actin (4967, Cell Signaling, 1:1000).

Tissue collection and histology

Gastrocnemius muscle was excised, weighted, frozen in isopentane cooled in liquid nitrogen, and stored at -80°C. Transverse sections (7μm) from the medial belly were cut on a cryostat and collected

on Superfrost plus glass slides. Cryosections were then processed for laminin staining. In detail, sections were fixed in 4% paraformaldehyde (PFA) for 10 min before being incubated with laminin antibody (1:200; Dako) and visualized by anti-mouse IgG Alexa Fluor 488 (Thermo Fisher Scientific) secondary antibody. Pictures of whole slides were acquired with the slide scanner Pannoramic Midi 1.14 (3D Histech, Budapest, Hungary) and cross sectional area (CSA) was measured automatically by ImageJ software.

Succinate dehydrogenase activity

Succinate dehydrogenase (SDH) enzymatic activity was determined on 15µm cryosections by specific staining (Bio-Optica, Milan, Italy) following the producer's instructions. Briefly, the cryosections were incubated with the rehydrated SDH solution for 45 min at 37°C, washed, fixed, and mounted on slides. Images were then acquired with the slide scanner Pannoramic Midi 1.14.

Cell culture and conditioned media (CM) preparation

C2C12 cells were cultured in DMEM /10% FBS and differentiated in DMEM/ 2% horse serum (HS) for 4 days as reported previously[25]. KPC cells were derived from a primary culture of pancreatic tumor cells of the Genetically Engineered Mouse Model of PDAC K-ras$^{LSL.G12D/+}$; p53$^{R172H/+}$; PdxCre mice (KPC).

Conditioned medium (CM) was prepared as following: KPC cells were grown in DMEM with 10% FBS supplemented with 1% penicillin and streptomycin. When cells reached full confluence, medium was removed; cells were washed twice with phosphate buffered saline (PBS) and once with serum-free DMEM. Cells were grown in serum-free DMEM for further 24h, then the medium was collected, centrifuged at 4000 rpm for 10 min, aliquoted, and stored at -80°C. Atrophy on C2C12 was induced with 10% CM treatment for 48h.

Myotube diameter quantification

C2C12 myotubes were treated with differentiation medium supplemented with 10% conditioned medium from KPC for 48 h. Pictures of myotubes were taken with bright field microscopy (Zeiss), and diameters of myotubes were measured using the software JMicroVision as previously described[25].

ROS measurement *in vitro*

ROS production was assessed in C2C12 myotubes by using the oxidant-sensitive fluorescent dye 29,79-dichlorodihydrofluoroscein diacetate (H_2DCFDA; Molecular Probes, Inc., Eugene, OR). Cells were incubated with 10 μM H_2DCFDA in PBS for 30 minutes at 37°C under 5% CO_2 atmosphere in darkness. Excess probe was washed out with PBS. Fluorescence was recorded at excitation and emission wavelengths of 485 nm and 530 nm, respectively, by a fluorescence plate reader (Promega). Fluorescence intensity was expressed as arbitrary units.

Mitochondria isolation

Mitochondrial fractions were isolated as previously reported[26], with minor modifications. Samples were lysed in 0.5 mL buffer A (50 mM Tris, 100 mM KCl, 5 mM $MgCl_2$, 1.8 mM ATP, 1 mM EDTA, pH 7.2), supplemented with protease inhibitor cocktail III (Calbiochem), 1 mM PMSF, and 250 mM NaF. Samples were clarified by centrifuging at 650 x *g* for 2 min at 4°C, and the supernatant was collected and centrifuged at 13,000 x *g* for 5 min at 4°C. This supernatant was discarded and the pellet containing mitochondria was washed in 0.5 mL buffer A and resuspended in 0.25 mL buffer B (250 mM sucrose, 15 mM K_2HPO_4, 2mM $MgCl_2$, 0.5 mM EDTA, 5% w/v BSA). A 50 μL aliquot was sonicated and used for the measurement of protein content or Western blotting; the remaining part was stored at -80°C.

Electron transport chain

The activity of Complex I–III was measured on 25 μL of non-sonicated mitochondrial samples resuspended in 145 μL buffer C (5 mM KH_2PO_4, 5 mM $MgCl_2$, 5% w/v BSA) and transferred into 96-well plate. Then, 100 μL buffer D (25% w/v saponin, 50 mM KH_2PO_4, 5 mM $MgCl_2$, 5% w/v BSA, 0.12 mM cytochrome c-oxidized form, 0.2 mM NaN_3) was added for 5 min at room temperature. The

reaction was started with 0.15 mM NADH and was followed for 5 min, the absorbance was measured at 550 nm by a Synergy HT Spectrophotometer (Bio-Tek Instruments). Under these experimental conditions, the rate of cytochrome c reduction, expressed as nmol cyt c reduced/min/mg mitochondrial proteins, was dependent on the activity of both Complex I and Complex III[27].

Intramitochondrial ATP levels

The amount of ATP was measured on 20 µg of mitochondrial extracts with the ATPlite assay (PerkinElmer), according to the manufacturer's instructions. Data were converted into nmoles/mg mitochondrial proteins, using a calibration curve previously set.

Intramitochondrial ROS levels

The amount of ROS in mitochondrial extracts was measured fluorimetrically incubating mitochondrial suspension at 37°C for 10 minutes with 10 µM of 5-(and-6)-chloromethyl-2,7-dichorodihydro-fluorescein diacetate-acetoxymethyl ester (DCFDA-AM), then washed and resuspended in 0.5 mL of PBS. Results were expressed as nmoles/mg mitochondrial proteins, using a calibration curve previously set with serial dilution of H_2O_2.

Fatty acids β-oxidation

Long-chain fatty acids were measured as described by Gaster et al[28] with minor modifications. 100 µl mitochondrial suspension were rinsed with 100 µl of 20 mM HEPES, containing 0.24 mM fatty acid-free BSA, 0.5 mM L-carnitine, and 2 µCi [1-^{14}C]palmitic acid (3.3 mCi/mmol, PerkinElmer). Samples were incubated at 37°C for 1 h, then 100 µl of 1:1 v/v phenylethylenamine 100 mM/methanol solution were added. After one hour at room temperature, the reaction was stopped by adding 100 µL of 0.8 N $HClO_4$. Samples were centrifuged at 13,000 x *g* for 10 min. Both the precipitates containing ^{14}C-acid soluble metabolites (ASM) and the supernatants containing $^{14}CO_2$-derived from oxidation (used as internal control and expected to be less than 10% of ASM) were counted by liquid scintillation. Results are expressed as nmol/min/mg cellular proteins.

Statistics

Statistical significance was evaluated with one-way or two-way analysis of variance (ANOVA) for multiple groups, followed by post-hoc test as defined in the figure legends. Student's unpaired t-test was used to compare two groups. All error bars indicate SEM. Significance was established as $P<0.05$. Data have been obtained from multiple independent experiments for *in vitro* assay and from at least 4 mice for *in vivo* experiments. All the analyses were performed with the software PRISM5 (GraphPad Software).

Discussion

Pancreatic cancer is a pathology with dismal prognosis associated with a stark decrease in quality of life, mostly because of cachexia development[29 30]. While cachexia is considered as the last step of cancer progression, it is important in PDAC to model the earliest steps of the disease (*i.e.*, pre-cachexia). Indeed, Mayers et al.[9] found that spontaneous PDAC mouse model presents an increased release of amino acids from the skeletal muscle months before the development of cachexia, which is consistent with data from PDAC patients[9]. These data advocate for the importance of defining alterations in skeletal muscle occurring in the early phases of disease, before the establishment of overt cachexia.

To this aim, we modified the cancer cachexia model described by Michaelis et al. to reproducibly induce cachexia with KPC cells[12]. Since KPC-bearing male mice present hormonal dysfunctions, we performed the study in female mice, although these animals are characterized by a moderate degree of wasting. While Michaelis and coworkers modeled cachexia by injecting up to 5×10^6 cells per mouse, thus promoting anorexia and subsequent animal death starting from 11-14 days, we injected only 0.7×10^6 cells (the minimal amount necessary to consistently promote tumor growth) in order to promote a slower tumor growth, thus allowing the characterization of pre-cachectic events. This reduced cell number resulted in barely palpable tumors at 2 weeks after injection (the time point where mice from Michaelis et al. already started to die of cachexia). Moreover, in contrast to the effects reported with

the injection of higher amount of KPC cells, smaller tumor mass (up to 75% reduction) and no effect on heart weight were observed (data not shown).

Despite the moderate degree of wasting, mice presented reduced muscle function and strength. In order to detect alterations in muscle morphology occurring at early phases of wasting, we sacrificed the mice at the first sign of decreased performance. At necropsy, mice presented a statistically significant reduction in gastrocnemius weight and fat deposit, but no signs of anorexia, excluding an involvement of food intake in the skeletal muscle mass reduction. Intriguingly, we found only a trend towards decreased body weight, similarly to the findings of Brown and colleagues[7]. Of note, it is known that many tumors hijack organ function, especially liver and spleen[3], by inducing increased organ size, which might counterbalance the drop in muscle and fat in the first phases. Muscle from tumor-bearing mice did not present any major transcriptional regulation of the investigated atrogenes. However, we identified increased levels of $AMPK^{T172}$ phosphorylation, indicative of ongoing energy stress, and protein ubiquitination indicating that the alterations present in muscle were mediated by a different pathway, *i.e.*, alternative ubiquitin ligase, a regulation at protein level, or alterations in protein deubiquitinases.

As previously shown in clear cell kidney cancer, muscle undergoing wasting is causally linked to increased fatty acid oxidation[16, 31], potentially raising noxious ROS generation in the mitochondria. Noteworthy, also in our model the significant drop in lipid was coupled with an increased fatty acid utilization and mitochondrial ROS generation, indicating a potential source of oxidative stress causing reduced muscular function and degeneration. Intriguingly, we identified an increased activity of SDH, uncoupled from increased ETC flux. Moreover, ATP content was decreased, suggesting a profound mitochondrial alteration. This observation further supports the concept that mitochondrial alterations occur at the early phases of cachexia. While SDH does not contribute to increasing mitochondrial energy metabolism in cachectic muscles, it promotes the metabolism of ketone bodies-derivatives that are produced in conditions of high fatty acid oxidation, *i.e.*, in the same metabolic conditions of KPC-bearing muscles. Redox cycles occurring at Complex I and Complex III of ETC are generally considered as the key sources of ROS within mitochondria[32]. However, also SDH complex has been recognized as an important source of intra-mitochondrial ROS[18]. Taken together, our findings suggest

that muscles consume fatty acids, forcing SDH activity in early cachexia. The final result is an energetic catastrophe that may severely impair muscle physiological performance.

Interestingly, *in vitro* myotubes did not show increased fatty acids oxidation during atrophy (not shown), in line with the fact that culture and differentiation media contain limited amount of fatty acids. However, C2C12 cells treated with the medium of pancreatic cancer cells displayed the same alterations observed in cachectic muscles, *i.e.*, high ROS levels and AMPK phosphorylation (not shown), suggesting that common metabolic alterations in mitochondrial metabolism occur in the early phase of cachexia both *in vitro* and *in vivo*.

In conclusion, we report a novel model of pre-cachexia causing a drastic reduction of muscle function and initial reduction of skeletal muscle mass. Interestingly, the onset of increased fatty acid oxidation and mitochondrial ROS generation occurs before the emergence of muscle mass reduction. Further test inhibiting fatty acid oxidation or mitochondrial ROS generation will be instrumental in understanding the relative contribution of such pathways to the pathogenesis of cachexia, as well as the identification of the factors secreted by PDAC cells causing muscle atrophy, both *in vitro* and *in vivo*.

Conflict of interest.

The author declares no conflict of interest.

Acknowledgements

PEP is supported by Italian Ministry for University and Research (MIUR, Rita Levi-Montalcini program for young researchers, 2014), NF is the recipient of a Fondazione Cariplo grant (2015-0634). We are grateful to Dr. Riccardo Taulli, Prof. Maurizio Giustetto and Prof. Stefano Geuna for helpful discussions and access to instrumentations, and to Erica Mina and Edoardo Ratto for valuable technical support.

LEGEND

Figure 1. Characterization of an *in vitro* and *in vivo* model of cancer-associated atrophy. C2C12 myotubes treated for 48 h with 10% conditioned medium (CM) from KPC cells. Dexamethasone (DEXA) was used as a positive control of atrophy induction. Pictures were acquired at the bright field microscope and (A) diameters were measured. (B) Increased ROS production in C2C12 myotubes treated with CM from KPC using oxidant-sensitive fluorescent dye H_2DCFDA. (C) No difference in food intake in tumor-bearing vs. control mice at the end of experiment, (D) no significant weight loss in KPC tumor-bearing vs. control mice. (E) Average tumor weight (Min Max Box Plot). Upon tumor growth at the end stage, mice presented reduced muscular resistance as evidenced by (F) performance at the hanging test (reach/fall assay) and (G) maximal strength as performed by grip test of upper-limbs. All experiments have been performed with $N \geq 4$ mice per group. All data are shown as means ± s.e.m; *n.s.*= non significant; * $P < 0.05$; *** $P < 0.001$; using one-way ANOVA with Bonferroni correction (A), Two-way ANOVA with Dunnett's multiple comparison test for (E), and Student T-Test for (B, C, D, F, and G).

Figure 2. KPC cell injection promotes skeletal muscle atrophy. (A) Gastrocnemius weight normalized on tibia length. (B) H&E representative pictures of muscle sections from control and KPC-injected mice. (C-E) Gastrocnemius myofiber membranes were stained for laminin, pictures of whole muscle section were acquired and cross sectional area (CSA) were measured (C). (D) Frequency histogram showing distribution of myofibers CSA in control and KPC-bearing mice. N = 4 (E) Representative pictures of laminin staining for CSA analysis in control and KPC-bearing mice. (F-I) KPC injection does not upregulate atrogene expression. $N \geq 4$. (J) Increased protein ubiquitination and AMPK (T172) phosphorylation in mice bearing tumor, blot representative of three independent experiments.

All data are shown as means ± s.e.m. Statistical analyses was conducted using two tailed t-test. *n.s.*= non significant.

Figure 3. Metabolic dysregulation of skeletal muscle in KPC-bearing mice. (A) Representative images for succinate dehydrogenase (SDH) activity stain. (B) Gastrocnemius mitochondria were isolated and ETC activity from Complex I to Complex III assessed by evaluating cytochrome C reduction. (C) ^{14}C-labeled palmitate was used as a substrate to measure Lipid Beta-Oxidation in isolated mitochondria of gastrocnemius from control and KPC-bearing mice. (D) Representative T_1-weighted MR images (brightest regions in T_1-weighted MR images correspond to adipose regions) and (E) in vivo measurement of adipose tissue using MR images in control group vs. KPC–bearing mice. (F) Weight of inguinal fat normalized on tibia length for control vs. KPC-bearing mice. (G) Gastrocnemius mitochondria were isolated and ATP level was assessed using ATPlite kit (Perkin Elmer, USA). (H) ROS measurement in isolated mitochondria from gastrocnemius using H_2DCFDA. $N \geq 4$. All data are shown as means ± s.e.m. Statistical analysis was conducted using two-tailed t-test. *n.s.*= non significant; * $P < 0.05$; ** $P < 0.01$; *** $P < 0.001$.

REFERENCES

1. Johns N, Stephens NA, Fearon KC. Muscle wasting in cancer. Int J Biochem Cell Biol 2013; 45:2215-29.

2. Tisdale MJ. Wasting in cancer. J Nutr 1999; 129:243S-6S.

3. Porporato PE. Understanding cachexia as a cancer metabolism syndrome. Oncogenesis 2016; 5:e200.

4. Fearon K, Strasser F, Anker SD, Bosaeus I, Bruera E, Fainsinger RL, Jatoi A, Loprinzi C, MacDonald N, Mantovani G, et al. Definition and classification of cancer cachexia: an international consensus. Lancet Oncol 2011; 12:489-95.

5. Lecker SH, Jagoe RT, Gilbert A, Gomes M, Baracos V, Bailey J, Price SR, Mitch WE, Goldberg AL. Multiple types of skeletal muscle atrophy involve a common program of changes in gene expression. FASEB J 2004; 18:39-51.

6. Marzetti E, Lorenzi M, Landi F, Picca A, Rosa F, Tanganelli F, Galli M, Doglietto GB, Pacelli F, Cesari M, et al. Altered mitochondrial quality control signaling in muscle of old gastric cancer patients with cachexia. Exp Gerontol 2017; 87:92-9.

7. Brown JL, Rosa-Caldwell ME, Lee DE, Blackwell TA, Brown LA, Perry RA, Haynie WS, Hardee JP, Carson JA, Wiggs MP, et al. Mitochondrial degeneration precedes the development of muscle atrophy in progression of cancer cachexia in tumour-bearing mice. J Cachexia Sarcopenia Muscle 2017.

8. Stewart GD, Skipworth RJ, Fearon KC. Cancer cachexia and fatigue. Clin Med (Lond) 2006; 6:140-3.

9. Mayers JR, Wu C, Clish CB, Kraft P, Torrence ME, Fiske BP, Yuan C, Bao Y, Townsend MK, Tworoger SS, et al. Elevation of circulating branched-chain amino acids is an early event in human pancreatic adenocarcinoma development. Nat Med 2014; 20:1193-8.

10. Bonetto A, Rupert JE, Barreto R, Zimmers TA. The Colon-26 Carcinoma Tumor-bearing Mouse as a Model for the Study of Cancer Cachexia. J Vis Exp 2016.

11. Narsale AA, Carson JA. Role of interleukin-6 in cachexia: therapeutic implications. Curr Opin Support Palliat Care 2014; 8:321-7.

12. Michaelis KA, Zhu X, Burfeind KG, Krasnow SM, Levasseur PR, Morgan TK, Marks DL. Establishment and characterization of a novel murine model of pancreatic cancer cachexia. J Cachexia Sarcopenia Muscle 2017.

13. Seto DN, Kandarian SC, Jackman RW. A Key Role for Leukemia Inhibitory Factor in C26 Cancer Cachexia. J Biol Chem 2015; 290:19976-86.

14. Reano S, Angelino E, Ferrara M, Malacarne V, Sustova H, Sabry O, Agosti E, Clerici S, Ruozi G, Zentilin L, et al. Unacylated Ghrelin Enhances Satellite Cell Function and Relieves the Dystrophic Phenotype in Duchenne Muscular Dystrophy mdx Model. Stem Cells 2017; 35:1733-46.

15. Segatto M, Fittipaldi R, Pin F, Sartori R, Dae Ko K, Zare H, Fenizia C, Zanchettin G, Pierobon ES, Hatakeyama S, et al. Epigenetic targeting of bromodomain protein BRD4 counteracts cancer cachexia and prolongs survival. Nat Commun 2017; 8:1707.

16. Fukawa T, Yan-Jiang BC, Min-Wen JC, Jun-Hao ET, Huang D, Qian CN, Ong P, Li Z, Chen S, Mak SY, et al. Excessive fatty acid oxidation induces muscle atrophy in cancer cachexia. Nat Med 2016; 22:666-71.

17. Hensley CT, Faubert B, Yuan Q, Lev-Cohain N, Jin E, Kim J, Jiang L, Ko B, Skelton R, Loudat L, et al. Metabolic Heterogeneity in Human Lung Tumors. Cell 2016; 164:681-94.

18. Balietti M, Fattoretti P, Giorgetti B, Casoli T, Di Stefano G, Solazzi M, Platano D, Aicardi G, Bertoni-Freddari C. A ketogenic diet increases succinic dehydrogenase activity in aging cardiomyocytes. Ann N Y Acad Sci 2009; 1171:377-84.

19. Edalat A, Schulte-Mecklenbeck P, Bauer C, Undank S, Krippeit-Drews P, Drews G, Dufer M. Mitochondrial succinate dehydrogenase is involved in stimulus-secretion coupling and endogenous ROS formation in murine beta cells. Diabetologia 2015; 58:1532-41.

20. Guaras A, Perales-Clemente E, Calvo E, Acin-Perez R, Loureiro-Lopez M, Pujol C, Martinez-Carrascoso I, Nunez E, Garcia-Marques F, Rodriguez-Hernandez MA, et al. The CoQH2/CoQ Ratio Serves as a Sensor of Respiratory Chain Efficiency. Cell Rep 2016; 15:197-209.

21. Indran IR, Tufo G, Pervaiz S, Brenner C. Recent advances in apoptosis, mitochondria and drug resistance in cancer cells. Biochim Biophys Acta 2011; 1807:735-45.

22. Geninatti-Crich S, Szabo I, Alberti D, Longo D, Aime S. MRI of cells and mice at 1 and 7 Tesla with Gd-targeting agents: when the low field is better! Contrast Media Mol Imaging 2011; 6:421-5.

23. Braccini L, Ciraolo E, Campa CC, Perino A, Longo DL, Tibolla G, Pregnolato M, Cao Y, Tassone B, Damilano F, et al. PI3K-C2gamma is a Rab5 effector selectively controlling endosomal Akt2 activation downstream of insulin signalling. Nat Commun 2015; 6:7400.

24. Perino A, Beretta M, Kilic A, Ghigo A, Carnevale D, Repetto IE, Braccini L, Longo D, Liebig-Gonglach M, Zaglia T, et al. Combined inhibition of PI3Kbeta and PI3Kgamma reduces fat mass by enhancing alpha-MSH-dependent sympathetic drive. Sci Signal 2014; 7:ra110.

25. Porporato PE, Filigheddu N, Reano S, Ferrara M, Angelino E, Gnocchi VF, Prodam F, Ronchi G, Fagoonee S, Fornaro M, et al. Acylated and unacylated ghrelin impair skeletal muscle atrophy in mice. J Clin Invest 2013; 123:611-22.

26. Campia I, Lussiana C, Pescarmona G, Ghigo D, Bosia A, Riganti C. Geranylgeraniol prevents the cytotoxic effects of mevastatin in THP-1 cells, without decreasing the beneficial effects on cholesterol synthesis. Br J Pharmacol 2009; 158:1777-86.

27. Wibom R, Hagenfeldt L, von Dobeln U. Measurement of ATP production and respiratory chain enzyme activities in mitochondria isolated from small muscle biopsy samples. Anal Biochem 2002; 311:139-51.

28. Gaster M, Rustan AC, Aas V, Beck-Nielsen H. Reduced lipid oxidation in skeletal muscle from type 2 diabetic subjects may be of genetic origin: evidence from cultured myotubes. Diabetes 2004; 53:542-8.

29. Fearon KC, Barber MD, Falconer JS, McMillan DC, Ross JA, Preston T. Pancreatic cancer as a model: inflammatory mediators, acute-phase response, and cancer cachexia. World J Surg 1999; 23:584-8.

30. Zhou X, Wang JL, Lu J, Song Y, Kwak KS, Jiao Q, Rosenfeld R, Chen Q, Boone T, Simonet WS, et al. Reversal of cancer cachexia and muscle wasting by ActRIIB antagonism leads to prolonged survival. Cell 2010; 142:531-43.

31. Mailloux RJ, Harper ME. Mitochondrial proticity and ROS signaling: lessons from the uncoupling proteins. Trends Endocrinol Metab 2012; 23:451-8.

FIG1.

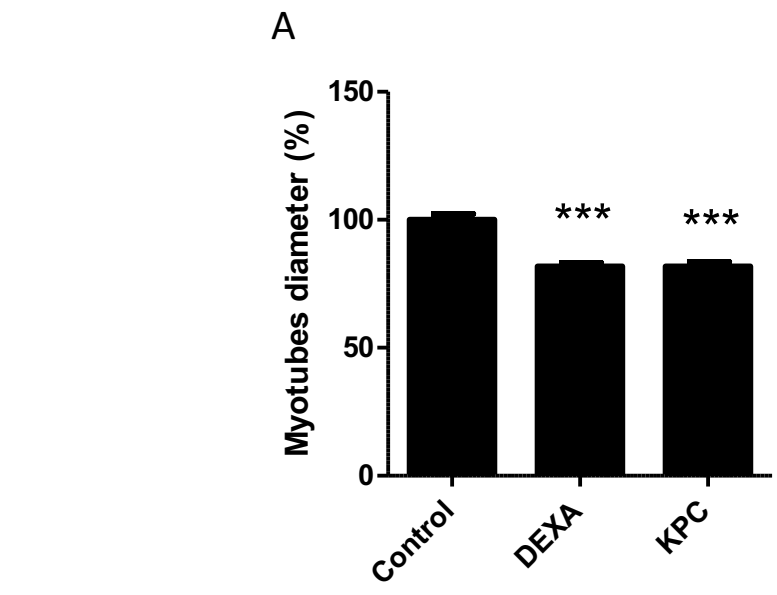
A
Myotubes diameter (%)
150
100
50
0
***
***
Control
DEXA
KPC

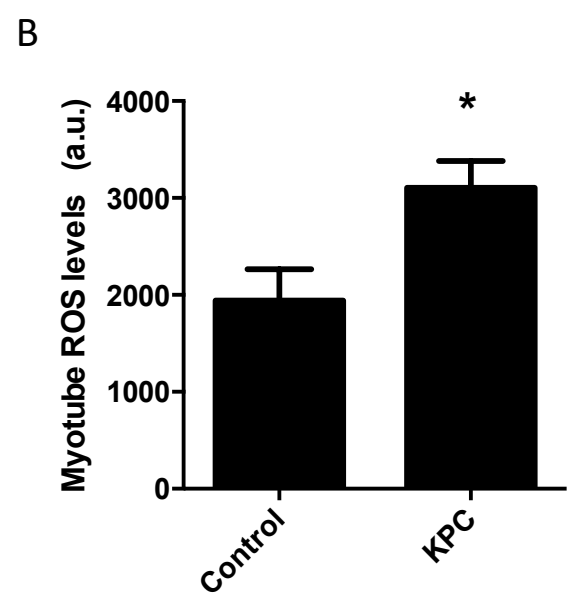
B
Myotube ROS levels (a.u.)
4000
3000
2000
1000
0
*
Control
KPC

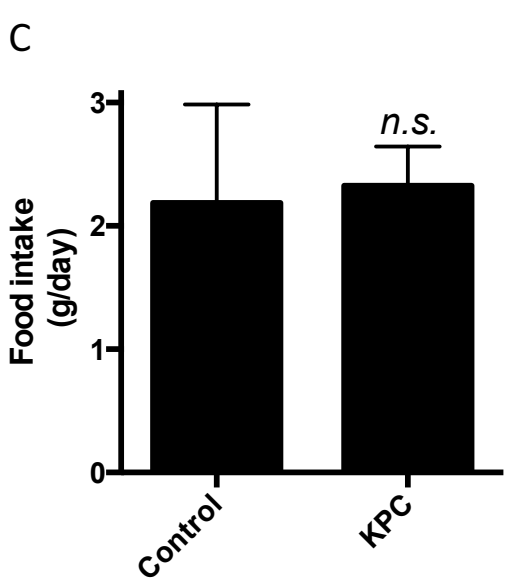
C
Food intake (g/day)
3
2
1
0
n.s.
Control
KPC

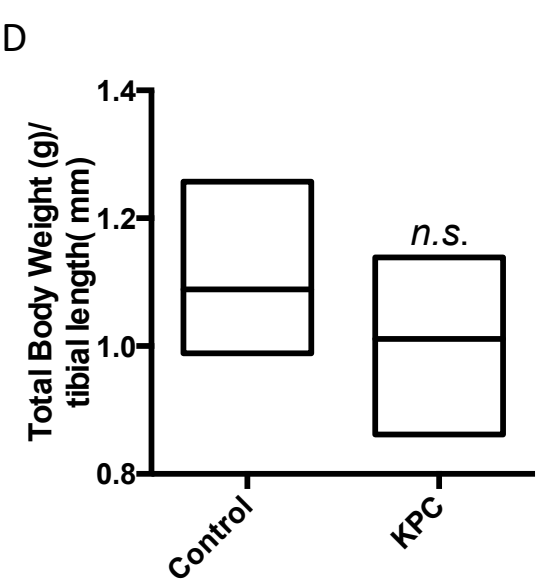
D
Total Body Weight (g)/ tibial length(mm)
1.4
1.2
1.0
0.8
n.s.
Control
KPC

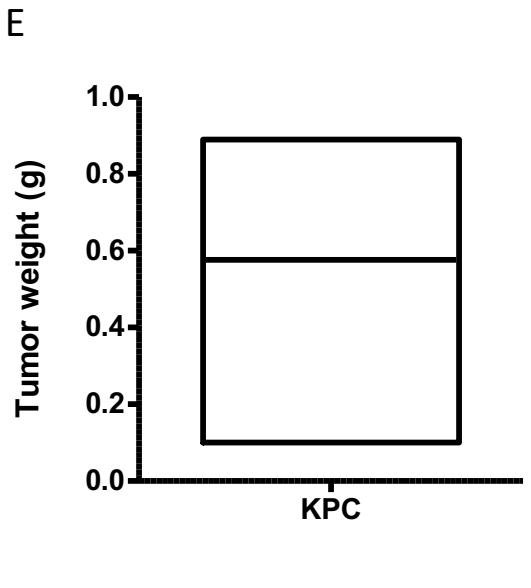
E
Tumor weight (g)
1.0
0.8
0.6
0.4
0.2
0.0
KPC

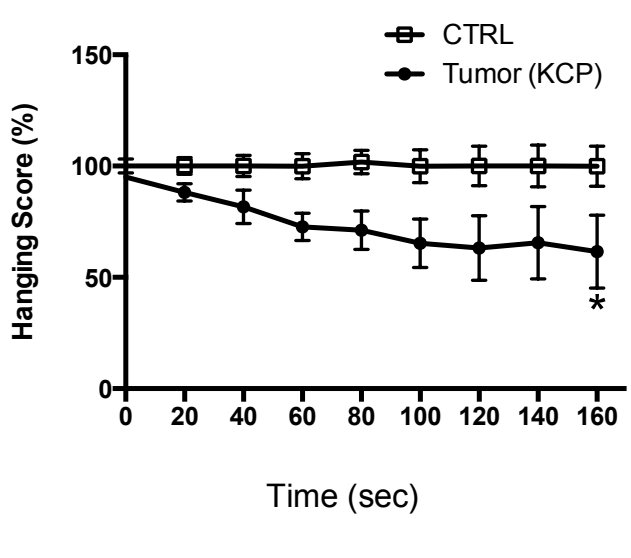
F
CTRL
Tumor (KCP)
Hanging Score (%)
150
100
50
0
0
20
40
60
80
100
120
140
160
*
Time (sec)

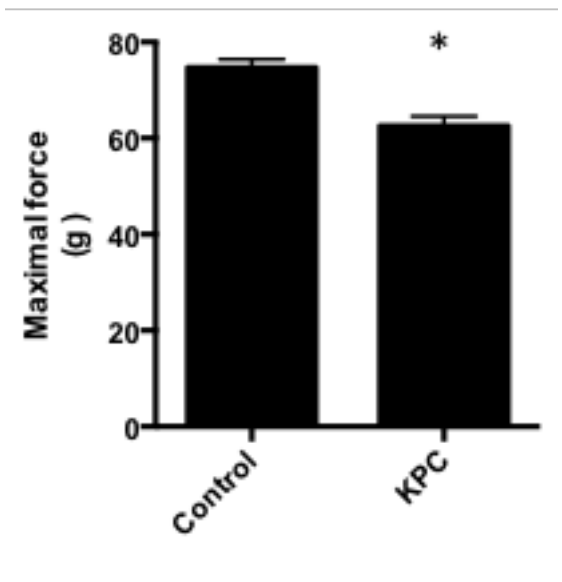
G
Maximal force (g)
80
60
40
20
0
*
Control
KPC

FIG2.

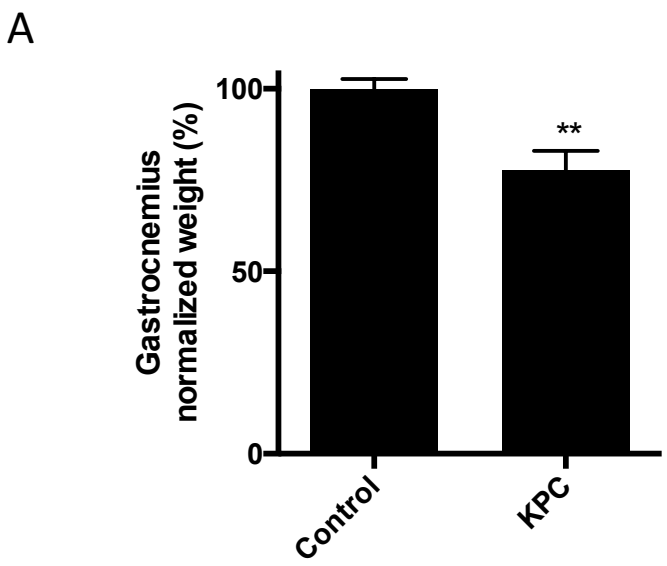
A
Gastrocnemius normalized weight (%)
100
50
0
**
Control
KPC

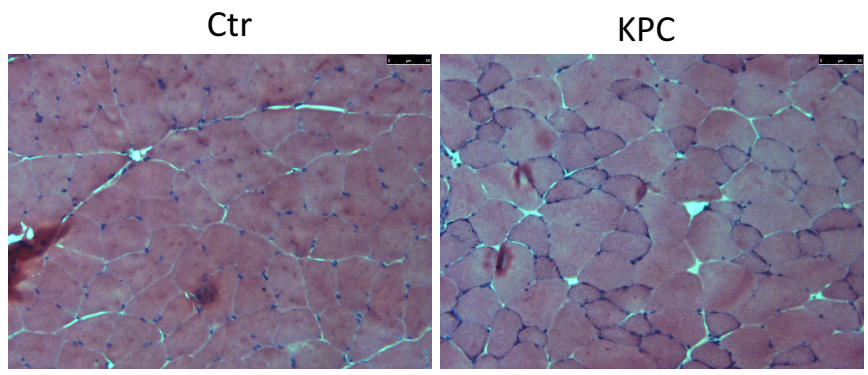
B
Ctr
KPC

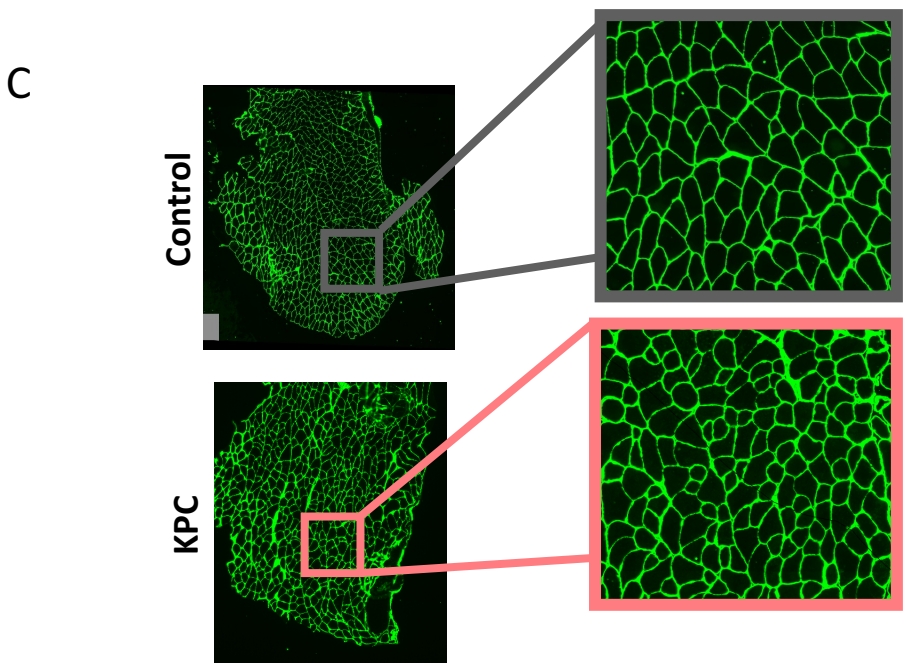
C
Control
KPC

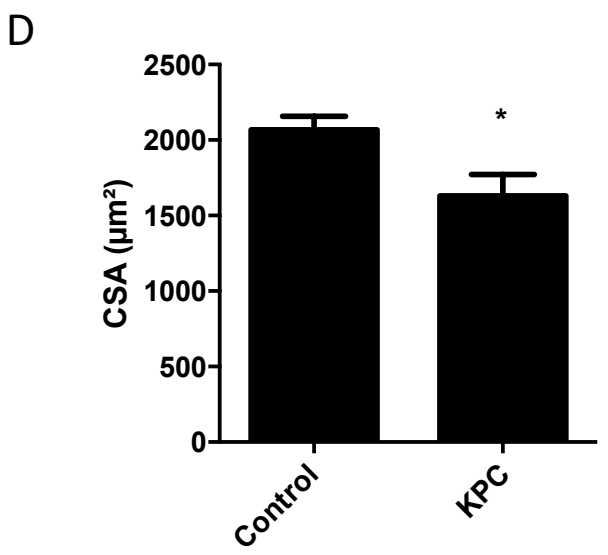
D
CSA (µm²)
2500
2000
1500
1000
500
0
*
Control
KPC

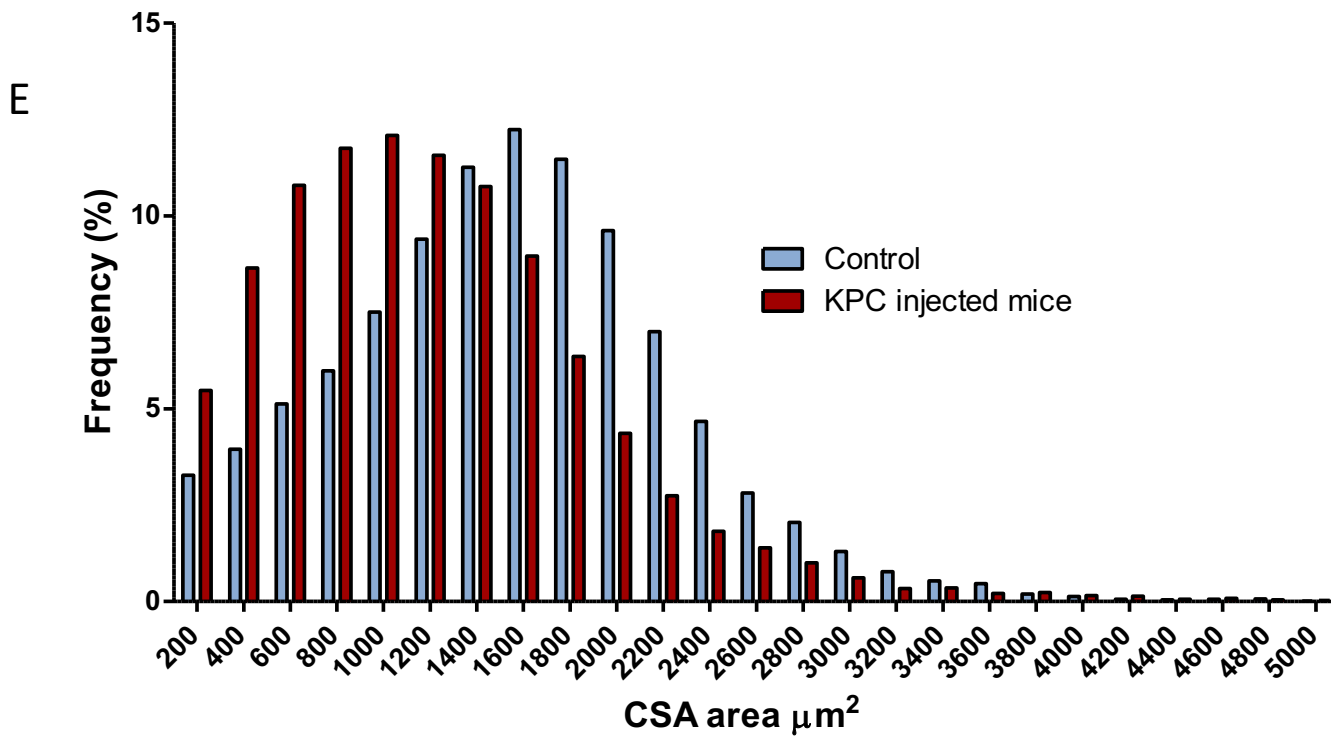
E
Frequency (%)
15
10
5
0
Control
KPC injected mice
200
400
600
800
1000
1200
1400
1600
1800
2000
2200
2400
2600
2800
3000
3200
3400
3600
3800
4000
4200
4400
4600
4800
5000
CSA area µm²

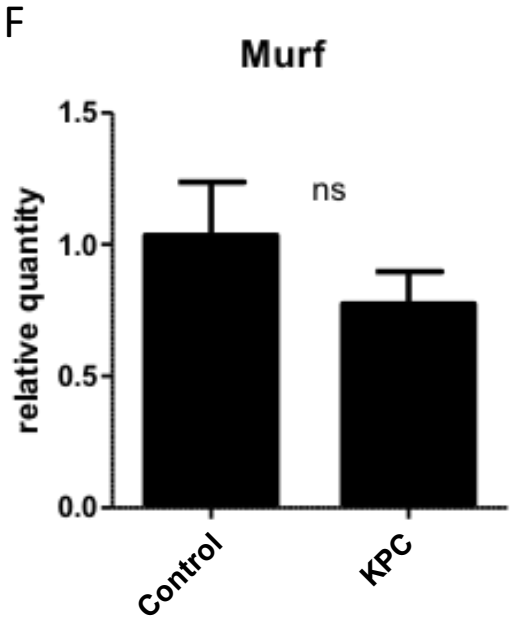
F
Murf
relative quantity
1.5
1.0
0.5
0.0
ns
Control
KPC

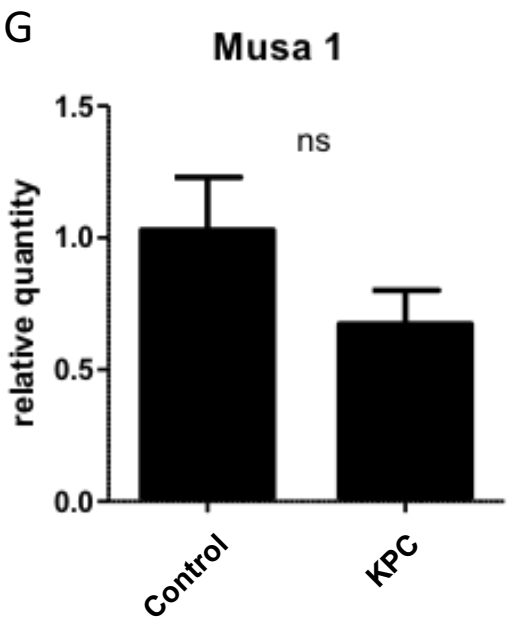
G
Musa 1
relative quantity
1.5
1.0
0.5
0.0
ns
Control
KPC

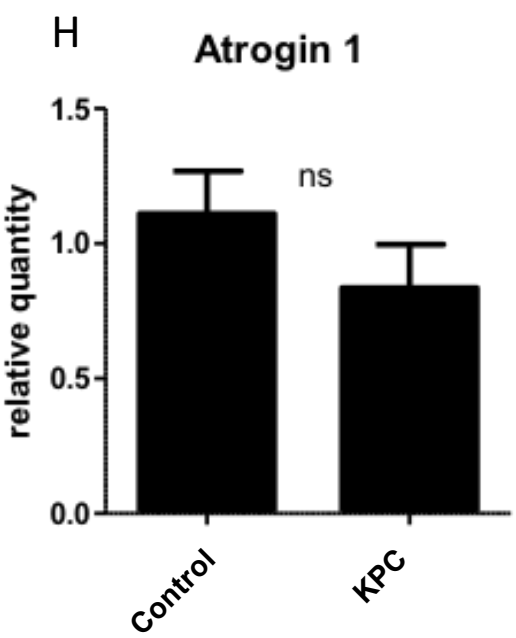
H
Atrogin 1
relative quantity
1.5
1.0
0.5
0.0
ns
Control
KPC

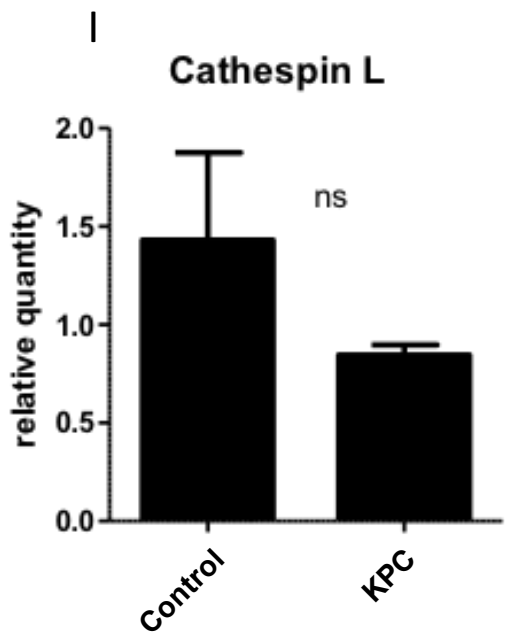
I
Cathespin L
relative quantity
2.0
1.5
1.0
0.5
0.0
ns
Control
KPC

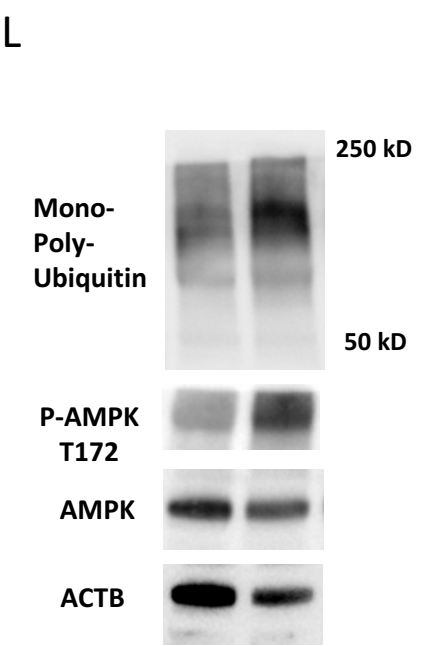
L
250 kD
Mono-
Poly-
Ubiquitin
50 kD
P-AMPK
T172
AMPK
ACTB
Control
KPC

FIG3. Metabolic dysregulation of sk.muscle in KPC-bearing mice

A

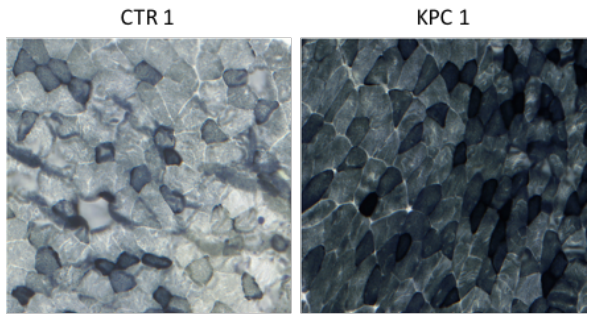

B

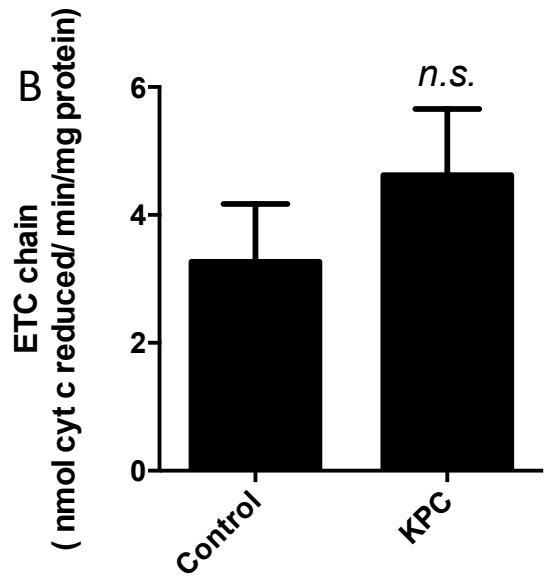

C

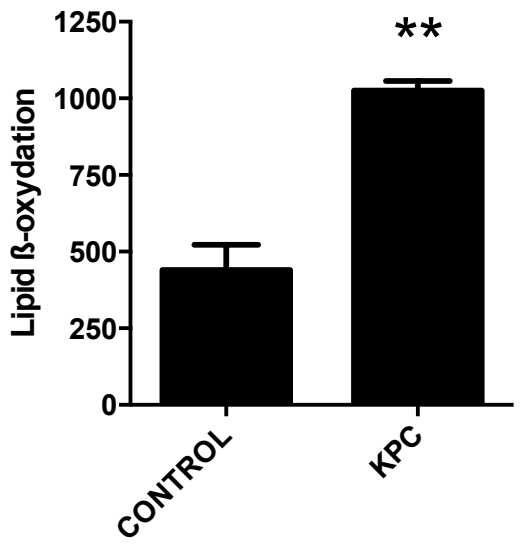

D

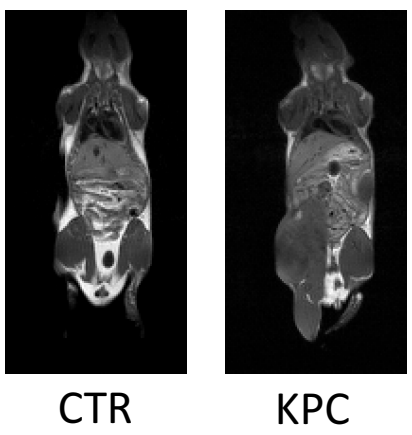

E

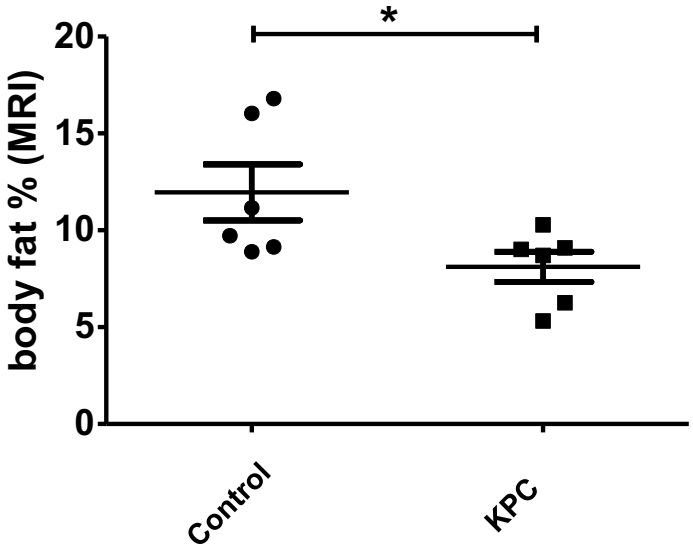

F

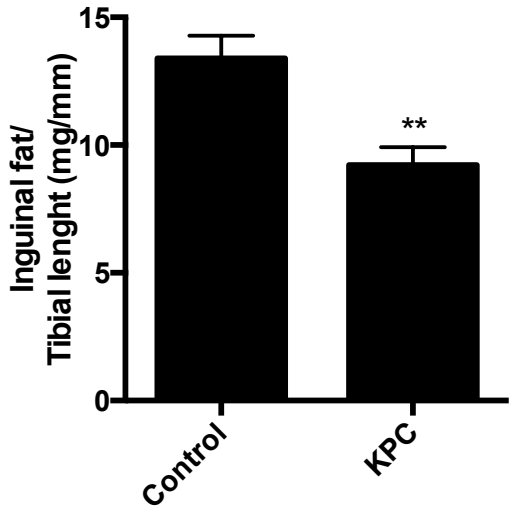

G

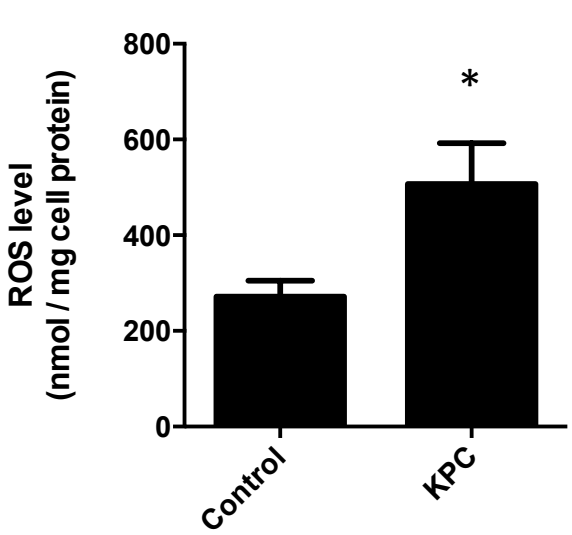

H